Asian Journal of Chemistry; Vol. 37, No. 3 (2025), 585-592

ASIAN JOURNAL OF CHEMISTRY

https://doi.org/10.14233/ajchem.2025.33192

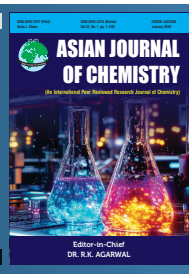

Luminescent Red Emitting Magnetic Fe_3O_4@$GdVO_4$:Eu^{3+} Nanocomposite: Heat Ability in AC Magnetic Field and Cell Viability in HCT116 Cell Lines

NEHRU S. KHUNDRAKPAM[1,*], BIKEN S. KHUNDONGBAM[1], IBOPISHAK S. OINAM[2], BIMOLA D. ASEM[3] and SOIBAM THOITHOISANA DEVI[4]

[1]Department of Chemistry, Manipur University, Canchipur, Imphal-795003, India
[2]Department of Chemistry, Modern College, Porompat, Imphal East-795005, India
[3]Department of Chemistry, Manipur College, Imphal East-795008, India
[4]Institute of Bio-resources and Sustainable Development (IBSD), Takyelpat, Imphal-795001, India

*Corresponding author: E-mail: khundrakpamnehru@gmail.com

Received: 13 December 2024; *Accepted*: 31 January 2025; *Published online*: 28 February 2025; AJC-21914

Red-emitting magnetic Fe_3O_4@$GdVO_4$:Eu^{3+} nanocomposite was synthesized to study its heat generation ability under the influence of alternating magnetic fields. The crystalline structure of the Fe_3O_4 and Fe_3O_4@$GdVO_4$:Eu^{3+} nanocomposite were confirmed and determined by X-ray diffraction (XRD) measurement. Fourier transformation infrared (FTIR) spectroscopy confirmed the presence of polyethylene glycol, from the solvent, adhered to the surface of the nanoparticles. From the TEM images, it is suggested that Fe_3O_4@$GdVO_4$:Eu^{3+} sample contains spherical (< 10 nm) and cubic (~100 nm) shaped particles. Vibrating sample magnetometry (VSM) analysis revealed the superparamagnetic nature of the sample with sufficient saturation magnetization (Ms) values and low coercivity (Hc) values. The samples were subjected to an alternating magnetic field showing efficient heat generation by the nanoparticles and the nanocomposites *viz*. 3.05×10^6 and 4.58×10^6 kAm^{-1} s^{-1}. The Fe_3O_4@$GdVO_4$:Eu^{3+} nanocomposite also showed strong red emission under excitation at 300 nm. The prepared nanocomposite was found to have high viability in HCT116 colon cancer cell lines. Therefore, Fe_3O_4@$GdVO_4$:Eu^{3+} magnetic luminescent nanocomposite may be useful for optical imaging and hyperthermia applications.

Keywords: Fe_3O_4 nanoparticles, Fe_3O_4@$GdVO_4$:Eu^{3+} nanocomposite, Optical imaging, Hyperthermia, HCT116 cell lines.

INTRODUCTION

Cancer is a leading cause of mortality globally, and a complete treatment is unattainable unless diagnosed in the early stages. However, it is challenging to diagnose cancer in its early stages. Nanotechnology provides a good opportunity for the diagnosis and treatment of cancer under hyperthermia, which involves heating specific organs or tissues to a temperature range of 41-46 ºC using small doses of magnetic nanoparticles [1-5]. Cancer cells can be killed when the temperature is raised to 42 ºC whereas normal cells can survive up to the temperature of 46 ºC, due to the cooling effect of blood circulation. Many researchers and scientists have made efforts for the improvement of hyperthermia techniques. The effective way of using hyperthermia for cancer treatment is to combine it with chemotherapy or radiotherapy which exhibits a significant reduction in side effects [6,7]. Few researchers [8,9] investigated the application of magnetic ferrofluids in hyperthermia treatment. The use of magnetic ferrofluids in hyperthermia is a promising technique for cancer treatment because of its ease in targeting the cancerous tissue and hence having fewer side effects than chemotherapy and radiotherapy [10].

Various researchers widely use gadolinium based luminescent phosphors in many fields [11]. $GdVO_4$ has good absorption in the ultraviolet region. The Gd^{3+} has excited state levels in the UV region (~270 nm) of relatively higher energy due to its half-filled ($4f^n$) ground state and the VO_4^{3-} has strong absorption around 280-400 nm [12,13]. The energy transfer from the host to Eu^{3+} ions through V–O charge transfer (CT) or Gd^{3+} ions excitation can lead to an efficient luminescence intensity of Eu^{3+} ions, which makes the $GdVO_4$:Eu^{3+} ions an efficient red light-emitting material [14]. Moreover, the paramagnetic

Gd^{3+} has a superior sensitivity to magnetic fields, rendering Gd^{3+}-based oxides and complexes more suitable for magnetic resonance imaging [15-18].

Magnetic nanoparticles (MNPs) have a variety of applications in biomedicine, like drug delivery, magnetic resonance imaging (MRI), hyperthermia, *etc*. [19-22]. Amongst the magnetic nanoparticles, ferrite nanoparticles are the most explored magnetic nanoparticles that enhanced their properties by clustering several individual superparamagnetic nanoparticles to form magnetic beads. Magnetic nanoparticles can bind to functional molecules and it allows transportation of drugs to a targeted location by applying an external magnetic field. To prevent aggregation and minimize the interaction between the nanoparticles with the system environment, surface coating of nanoparticles is required [23]. The surface of ferrite nanoparticles can be modified by using surfactants, silica or phosphoric acid derivatives to increase their stability in solution. Such surface coated magnetic nanoparticles are widely used in various medical applications, like cell isolation, drug delivery, immunoassay, diagnostic testing and targeted therapeutic [24].

The magnetic-luminescent nanocomposites can be applicable in hyperthermia for cancer therapy. Since Fe_3O_4 nanoparticles alone do not show any luminescence properties they are not suitable for bioimaging purposes. When mixed with luminous materials, it becomes readily visible; nevertheless, in the absence of luminescent properties, tracing Fe_3O_4 nanoparticles during hyperthermia administration within the human body proves to be exceedingly challenging. Such prepared nanocomposite has both properties of luminescence and magnetism. Here, Fe_3O_4 gives the necessary heat for hyperthermia application and inorganic phosphor gives the required luminescence for bioimaging purposes [25-27].

By utilizing MNPs, which can elevate the hyperthermia temperature, magnetic hyperthermia seeks to offer a safe, effective and simple therapeutic option. Use of MNPs in the hyperthermia treatment dominance to differentiate temperature profile of healthy tissues and tumor that inject MNPs into small areas [28]. Magnetic nanoparticles (MNPs) also play an important role in transforming energy into heat by absorbing AC magnetic field. When an external AC magnetic field is applied to the targeted location which is made by injecting MNPs, a limited amount of heat is produced and driven throughout the tissue. Fe_3O_4 based magnetic nanocomposites showed promising potential for hyperthermia application that can be evacuated by the body after some weeks without any toxicity [29,30]. Preparation of MNPs with multi-functional properties and surface functionalized, which can show the highest saturation magnetization is of utmost importance [23]. Surface functionalization of the magnetic luminescent nanomaterials is required to improve the chemical and physiological stability as well as bioadhesion [31,32].

Superparamagnetic iron oxide nanoparticles (SPIONs) are focused in the field of hyperthermia applications due its the potentiality to be directed by an AC magnetic field to specifically target the tumor regions and to dissipate heat locally, with negligible agglomeration among particles [33,34]. The heating efficacy of SPIONs, expressed in terms of specific absorption rate (SAR) is a pivotal factor determining the success of hyperthermia applications. A higher value of SAR leads to the high efficiency of magnetic fluid hyperthermia (MFH), measured by the specific absorption rate (SAR) with the shortest duration of treatment and reducing the toxic effects of magnetic nanoparticles [35,36]. The SAR value is consequently calculated in terms of the effective relaxation time, $\tau_{effective}$. For maximum SAR, the optimization of surface coating on MNPs based hyperthermia is a crucial factor. For instance, the highest SAR in magnetic fluid hyperthermia (MFH) was achieved using PEG coated Fe_3O_4 NPs [37]. Such optimized coated nanoparticles have also exhibited excellent hyperthermic activity in both water and simulated body fluids.

Herein, polyethylene glycol 4000 (PEG 4000)-coated Fe_3O_4 and magnetic luminescent nanocomposite Fe_3O_4@$GdVO_4$:Eu^{3+} were synthesized to study their heat generation ability under the influence of alternating magnetic field. The samples exhibited excellent response under the influence of alternating magnetic fields. They generate more than sufficient amount of heat required for killing cancerous cells. The nanocomposite showed good viability to HTC116 colon cancer cell lines. The results show that the nanocomposites can be potential candidates for magnetic fluid hyperthermia and optical imaging.

EXPERIMENTAL

Anhydrous iron(III) chloride ($FeCl_3$, 99.9%, Merck), iron(II) chloride tetrahydrate ($FeCl_2{\cdot}4H_2O$, Merck), gadolinium acetate hydrate ($Gd(CH_3CO_2)_3$, 99.9%, Sigma-Aldrich), europium(III) oxide (Eu_2O_3, 99.9%, Sigma-Aldrich), ammonium meta vanadate (NH_4VO_3, 99%, Sigma-Aldrich), polyethylene glycol 4000 ($H(OCH_2CH_2)_nOH$, Merck), lithium hydroxide, (LiOH, 98%, Sigma Aldrich), conc. HCl (37%, Merck), conc. HNO_3 (70%, Merck) and deionized water were used. All chemicals were used analytically pure without further purification.

Synthesis of Fe_3O_4 nanoparticles: In order to synthesize **Fe_3O_4** nanoparticles, a solution containing 150 mL of distilled water and 7.5 g of PEG 4000 was heated at 50 ºC with constant stirring for 30 min followed by the addition of 1.4910 g of $FeCl_2{\cdot}4H_2O$ with continuous stirring for 15 min. Then, 2.433 g of $FeCl_3$ was added while stirring for 30 min thereafter conc. HCl was added till the solution becomes pale yellow and magnetic stirring was continued for another 10 min. Finally, 3.147 g of LiOH was added with constant stirring for 1 h and allowed to settle for overnight. The black precipitate was concentrated by magnetic decantation and the supernatant liquid was removed using a micropipette. This process was repeated for 5 times (upto the pH is neutral), collected the black precipitate by centrifugation, washed with water, dispersed in acetone for about 12 h and finally collected using a magnet. The black product was dried at 40 ºC overnight and then ground to fine powder.

Synthesis of Fe_3O_4@$GdVO_4$:Eu^{3+} (5 at.%): Eu_2O_3 (0.0176 g) was dissolved in 40 mL conc. HNO_3. The excess acid was removed by evaporating it with distilled water. Then, 0.6354 g $Gd(CH_3CO_2)_3$ and 20 mL of distilled water were added with constant magnetic stirring followed by the addition of 40 mL of glycol and 60 mL of water. The mixture was continually stirred with a magnetic stirrer for approximately 1 h, after which

0.2342 g of NH_3VO_4 was added and the magnetic stirring continued for 24 h to obtain a green colour solution. To this solution, 300 mg of Fe_3O_4 (sample prepared) was added and magnetic stirring continued for 1 h. To this black solution, a mixture of 0.4200 g LiOH + 10 mL glycerol + 20 mL distilled water was added and continued stirring for 30 min, heated for 15 min, refluxed for 2 h at 160 ºC and thne centrifuged at 845 rpm. The collected precipitate was kept for further analysis.

Characterization: Fourier transform infrared (FT-IR) spectroscopy was used to identify the functional groups present in the prepared sample using Perkin-Elmer spectrum two (FT-IR). The spectra were recorded in the range of 4000–400 cm^{-1} in the transmittance mode. Transmission electron microscope (TEM, JEOL JEM-2100, Japan) operated at 200 kV was used for studying the shape and size of the materials. The photoluminescence (PL) spectra and lifetimes of these powder phosphors were recorded using a Hitachi F-7000 FL spectrophotometer equipped with a 150 W Xenon lamp as a source. All of the measurements were carried out at room temperature. The iron contents in the nanocomposites were determined by inductively coupled plasma optical emission spectroscopy using a Perkin-Elmer OPTIMA 5300 DV ICP-OES operating in the range of 165-782 nm. The X-ray analysis of the prepared nanoparticles were measured by using a PAN-alytical powder X-ray diffractometer (X-Pert-PRO) equipped with a Cu$K\alpha$ (1.5406 Å) radiation source and Ni filter. Unit cell parameters were calculated using the Unit Cell Program (rTim Holland and Simon Redfern). The crystallites size (d) was calculated using the Scherrer's equation:

$$d = \frac{0.94\lambda}{\beta\cos\theta}$$

where λ is the wavelength of the X-ray beam, β is the full width at half maximum (FWHM) of a diffraction peak and θ is the diffraction angle.

The magnetic measurements were carried out by using vibrating sample magnetometer (VSM) at room temperature using a Lakeshore VSM 7410 instrument in an applied magnetic field of ± 1.5 T. The magnetization studies are performed in the powder state. The measurements of the induction heating ability of the magnetic nanoparticles and nanocomposites were performed using Easy Heat 8310, Ambrell, U.K. The instrument was equipped with induction coils and a provision for water circulation through their coils in order to maintain ambient temperature. The sample suspended in 1 mL of deionized water was taken in a 1.5 mL micro-centrifuge tube and this was placed at the centre of the coil without touching the walls. The sample was heated using a current of 300 A up to 10 min (600 s). The resultant magnetic field (H) generated due to the applied current (i) was calculated using the following relation:

$$H = \frac{1.257ni}{D}(Oe)$$

where n is the number of turns in the coil and D is the diameter of the turn in cm. The magnetic field intensity is then converted to kA m^{-1} s^{-1} units to compare with the clinical threshold of magnetic field intensity. The temperature of the system, where the sample was kept in the centre of coil was recorded using an optical temperature sensor (Photon R & D, Canada) with the accuracy of ± 0.01 ºC. A copper (Cu) coil has a frequency of f = 178 kHz, which corresponds to the measurement window time of 5.6×10^{-6} s. The coil of diameter (D) = 7 cm, numbers of turns (n) = 6 and its operating frequency (f) = 178 kHz generated two magnetic field strengths (Hf) of 3.05×10^6 and 4.58×10^6 kA m^{-1} s^{-1} when 200 and 300 A current were respectively passing through the coil. The sample concentrations of 2, 5, 10, 15 and 20 mg of the magnetic-luminescent nanocomposites dispersed in 1 mL of deionized water were measured for their heat generation efficiency.

MTT cell viability assay: Cancer cells (HCT116 cell line) were seeded on 96-well plate at 5×10^3 to 7×10^3 cell per well. After the attachment of the cells (after 24 h of incubation), the old media was discarded and the cells were treated at concentration gradient of 7 µg/mL to 500 µg/mL. The plates were then incubated for 48 h in 5% CO_2 incubator at 37 ºC. Then, 20 µL of MTT dye solution (5 mg/mL) was added to each well and left in incubator for 4 h. After the incubation all the media were removed carefully and the formazan was solubilized using DMSO. The solubilization solution (DMSO, 100 µL) was added to each well and the absorbance at wavelength of 570 nm in a microplate reader was noted. The quantity of formazan produced (as measured by the absorbance at 570 nm) is directly proportional to the number of living cells [27]. The absorbance of the treated cells was compared with that of the control. The experiments were conducted in triplicate wells and repeated twice. The IC_{50} was determined using GraphPad Prism.

RESULTS AND DISCUSSION

XRD studies: Fig. 1a shows the X-ray diffraction (XRD) patterns of Fe_3O_4 nanoparticles obtained in the 20º to 70º range in 2θ. The diffraction patterns of Fe_3O_4 can be indexed well to the cubic phase in accordance with the reference JCPDS 85-1436. The calculated lattice parameter (a) and unit cell volume (V) of Fe_3O_4 nanoparticles are a = 8.394 Å and V = 591.29 $Å^3$. The crystallite size calculated using Scherrer formula from the (311) peak is found to be 7.4 nm. Fig. 1b shows the X-ray diffraction (XRD) patterns of Fe_3O_4@$GdVO_4$:Eu^{3+} nanocomposite. The asterisks (*) in the figure denote the diffraction peaks of the Fe_3O_4 cubic phase and the strong diffraction peaks at 24.65º in 2θ is *i.e.* (200) plane is from the tetragonal phase of $GdVO_4$:Eu^{3+}. The diffraction patterns of $GdVO_4$:Eu^{3+} match well with the tetragonal crystalline structure in accordance with the JCPDS card No. 72-0277. The lattice parameter (a) and unit cell volume (V) of Fe_3O_4 nanoparticles are a = 7.218 Å, c = 6.340 and V = 330.38 $Å^3$, respectively. The crystallite size calculated from (200) peak is found to be 53.3 nm. In the diffraction pattern of nanocomposite, the peaks due to the cubic phase of the Fe_3O_4 component cannot be observed distinctly. This could be due to the small size of the Fe_3O_4 nanoparticles, which could give low intensity peaks and the larger $GdVO_4$:Eu^{3+} dominates the diffraction peaks.

Elemental analysis: The estimation of Fe content by ICP analysis found that 8.5 mg of Fe_3O_4@$GdVO_4$:Eu^{3+} nanocomposite contained 33.99 wt.% (57.78 ppm). The diluter factor

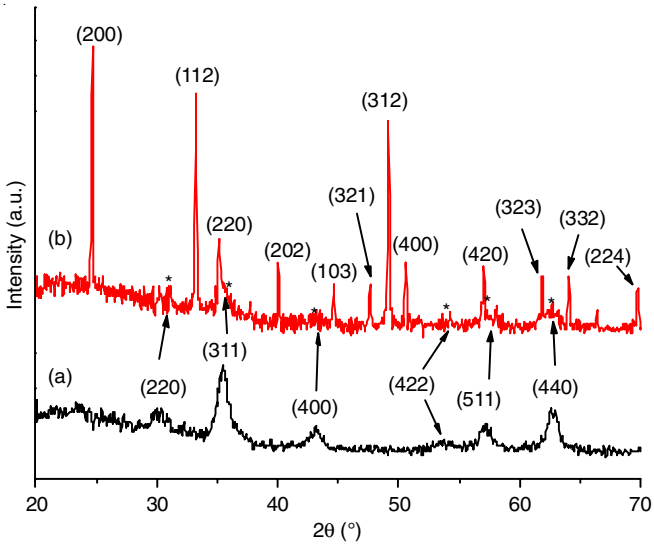

Fig. 1. X-ray diffraction patterns of the (a) Fe_3O_4 nanoparticles and (b) Fe_3O_4@$GdVO_4$:Eu^{3+} nanocomposite. The asterisk in (b) denotes the cubic phase due to the Fe_3O_4 nanoparticles in the nanocomposite

is 1 and the value is 50 mL. This wt.% corresponding to 2.89 mg of Fe *i.e.* 3.99 mg of Fe_3O_4 approximately.

FTIR spectral studies: In, Fig. 2a, the FTIR peak at 659 cm^{-1} corresponds to Fe–O vibration, whereas the peak at 1617 cm^{-1} corresponds to O–H bending vibration and the broad peak around 3470 cm^{-1} corresponds to stretching vibration of O–H. The vibrational due to the CH_2 groups of polyethylene glycol molecule can be observed as weak bands in the 2900-2840 cm^{-1} region. This indicates the coating of the Fe_3O_4 nanoparticles by the polymer on its surfaces. In Fig. 2b, the FTIR spectrum of Fe_3O_4@$GdVO_4$:Eu^{3+} nanocomposite is shown. The Fe–O and the V–O stretching modes can be observed at about 611 and 865 cm^{-1}, respectively [13,14]. The peaks in the 1760-1290 cm^{-1} region correspond to the CH_2 deformation. And the CH_2 stretching vibrations are observed in the 2900-2840 cm^{-1} cm^{-1} region, whereas the presence of O–H can be justified by the broad peaks centered at 3452 cm^{-1}.

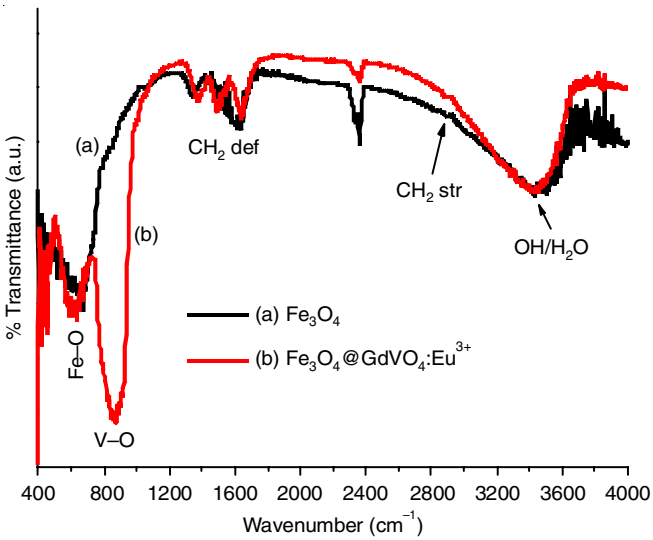

Fig. 2. FTIR spectra of the (a) Fe_3O_4 nanoparticles and (b) Fe_3O_4@$GdVO_4$:Eu^{3+} nanocomposite

TEM study: The TEM images of the Fe_3O_4@$GdVO_4$:Eu^{3+} nanocomposite are shown in Fig. 3a-c. It is observed that the sample consists of particles of mainly two different sizes. The particles with smaller dimensions less than 10 nm are the Fe_3O_4 nanoparticles, whereas the particles of nearly 100 nm in size are the $GdVO_4$:Eu^{3+} nanoparticles. It was also observed that the magnetic Fe_3O_4 and the luminescent $GdVO_4$:Eu^{3+} nanoparticles are adhered to one another. This provides the multimodality of the magnetic-luminescent nanocomposites. Fig. 3d shows the selected electron diffraction (SAED) pattern of the Fe_3O_4@$GdVO_4$:Eu^{3+} nanocomposite. Rings of bright spots can be observed, which indicates the well crystalline nature of the nanocomposite.

VSM analysis: Fig. 4 shows the magnetization (M) *versus* applied magnetic field (H) for the Fe_3O_4 nanoparticles and Fe_3O_4@$GdVO_4$:Eu^{3+} nanocomposite. The saturation magnetization (Ms) of the samples is calculated from the linear fitting of the plot of M *versus* 1/H since the superparamagnetic iron oxide nanoparticles do not acquire saturation of the magnetization for the applied magnetic field upto 1.5×10^4 Gauss. The magnetization retentivity (M_r) and the coercivity (H_c) of the samples are reported as obtained from the measurement. The Fe_3O_4 nanoparticles exhibit the M_s, M_r and H_c values of 56.52 emu/g, 3.00 emu/g and 58.76 Gauss respectively. The M_s value for the Fe_3O_4 is sufficiently high and it suggests a good response towards the application of an external magnetic field. The low M_r value also suggests the quick loss of magnetization once the external applied magnetic field is removed. The Fe_3O_4@$GdVO_4$:Eu^{3+} nanocomposites exhibit the M_s, M_r and H_c values of 24.09 emu/g, 0.77 emu/g and 40.48 Gauss, respectively. The M_s and the M_r values for the nanocomposite are relatively lowered due to the decreased content of Fe_3O_4. However, it still suggests a good response is exhibited to the applied magnetic field. Here, both the nanoparticles and the nanocomposites do not exhibit zero H_c values. This could be because of the slight agglomeration of the magnetic nanoparticles. Otherwise, the H_c value will be zero for ideal superparamagnetic nanoparticles. The application of such magnetic nanoparticles or the magnetic-luminescent nanocomposites for hyperthermia must have the ability to generate efficient heat dissipation within the limits of strength and frequency of the magnetic field. The ability of the heat dissipation is strongly dependent on the response of the magnetic nanoparticles towards the external magnetic field. Since the Fe_3O_4 nanoparticles and Fe_3O_4@$GdVO_4$:Eu^{3+} nanocomposite show good magnetization responses, these materials will be potential candidates for magnetic fluid hyperthermia.

Induction heating studies: The induction heating measurements were carried out for surface modified Fe_3O_4 nanoparticles under different current strengths (200 A and 300 A) for 10 min. The magnetic nanoparticle suspensions were prepared by dissolving 2.5, 10, 15 and 20 mg of magnetic samples in 1 mL of distilled water. The heating ability of the magnetic nanoparticles was found dependent on its concentration and current applied. For each concentration, the time required to increase the temperature decreases as the current strength increases. Specifically, between 41 and 46 ºC, the hyperthermia temperature, was efficiently attained at current intensities of 200 A and 300 A.

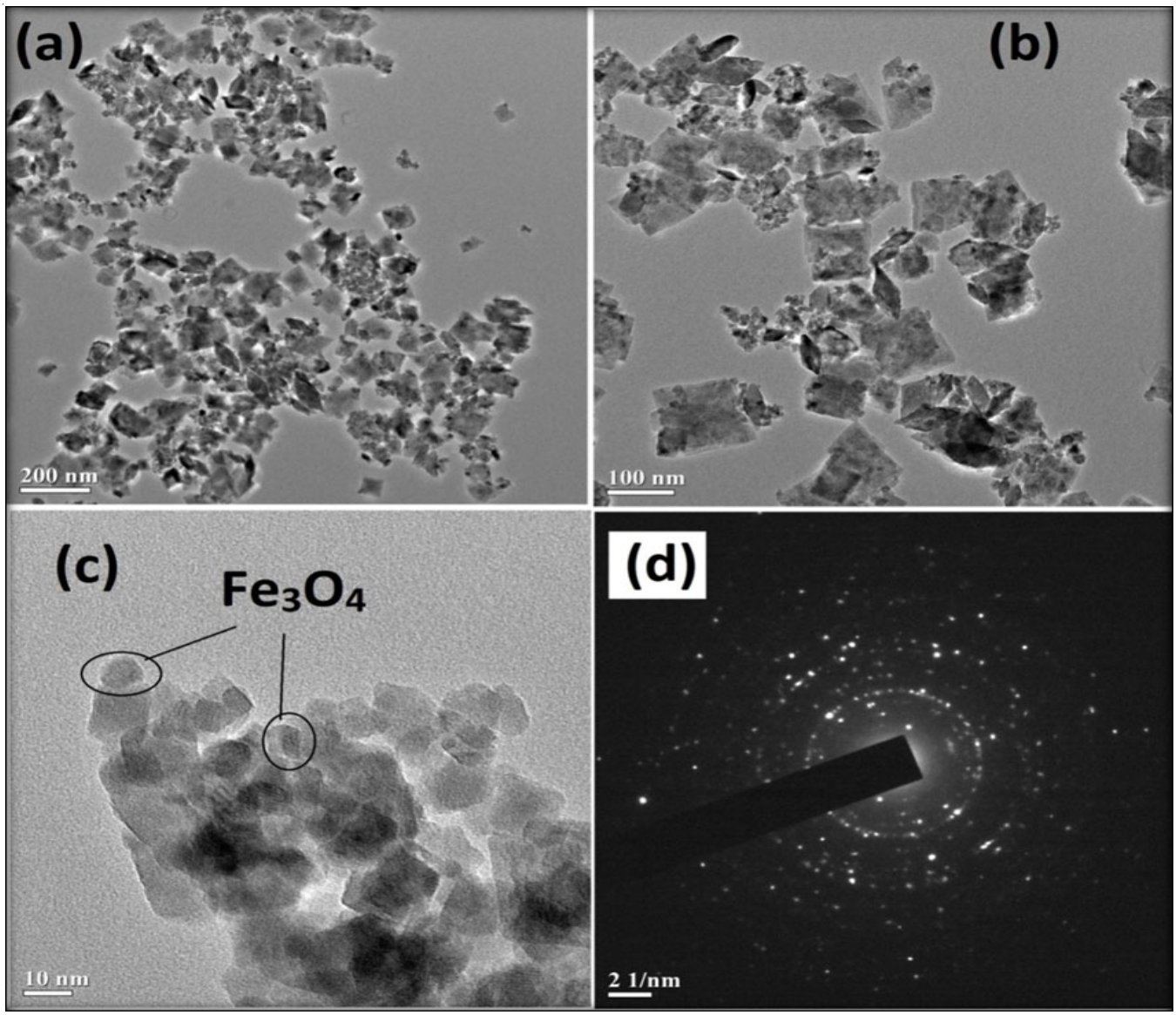

Fig. 3. (a,b,c) TEM images and (d) selected are electron diffraction (SAED) pattern of the Fe_3O_4@$GdVO_4$:Eu^{3+} nanocomposite

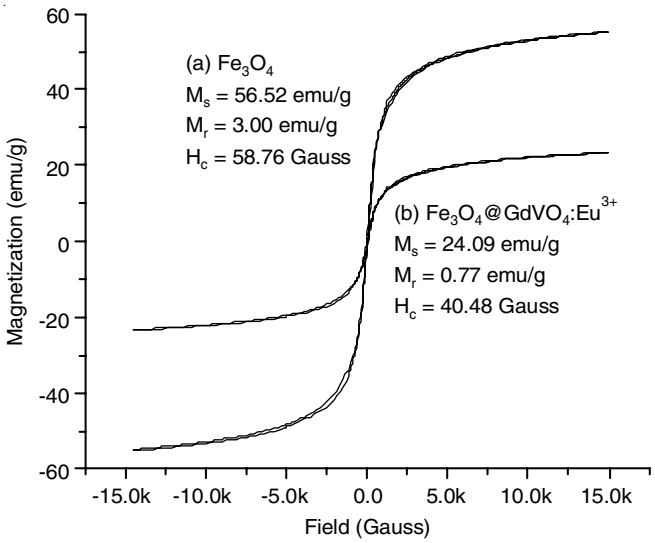

Fig. 4. Plot of magnetization *versus* applied magnetic field for the (a) Fe_3O_4 nanoparticles and (b) Fe_3O_4@$GdVO_4$:Eu^{3+} nanocomposite

A current over 400A is unsustainable due to the excessive heat generated in the coil, which surpasses the physiological temperature (37 ºC). The generation of heat from the Fe_3O_4 sample at 200 A current strength is shown in Fig. 5a. It was observed that at 200 A, the slopes of each temperature *versus* time plot increase with increasing Fe_3O_4 concentration.

At 200 A, it is observed that 2 mg and 5 mg content samples were not able to achieve hyperthermia temperature. Whereas 10 mg content sample can generate the hyperthermia temperature. Moreover, 15 and 20 mg contents of samples can also achieved hyperthermia temperature in a shorter duration in applying magnetic field. On increasing the sample to 15 mg and 20 mg, the rate of heat generation increases faster. This result suggests the advantages of current strength dose dependent application.

The similar patterns of slopes were found at 300 A current, the slopes of each temperature *versus* time plots increase with increasing Fe_3O_4 concentration (Fig. 5b). Additionally, 2 mg

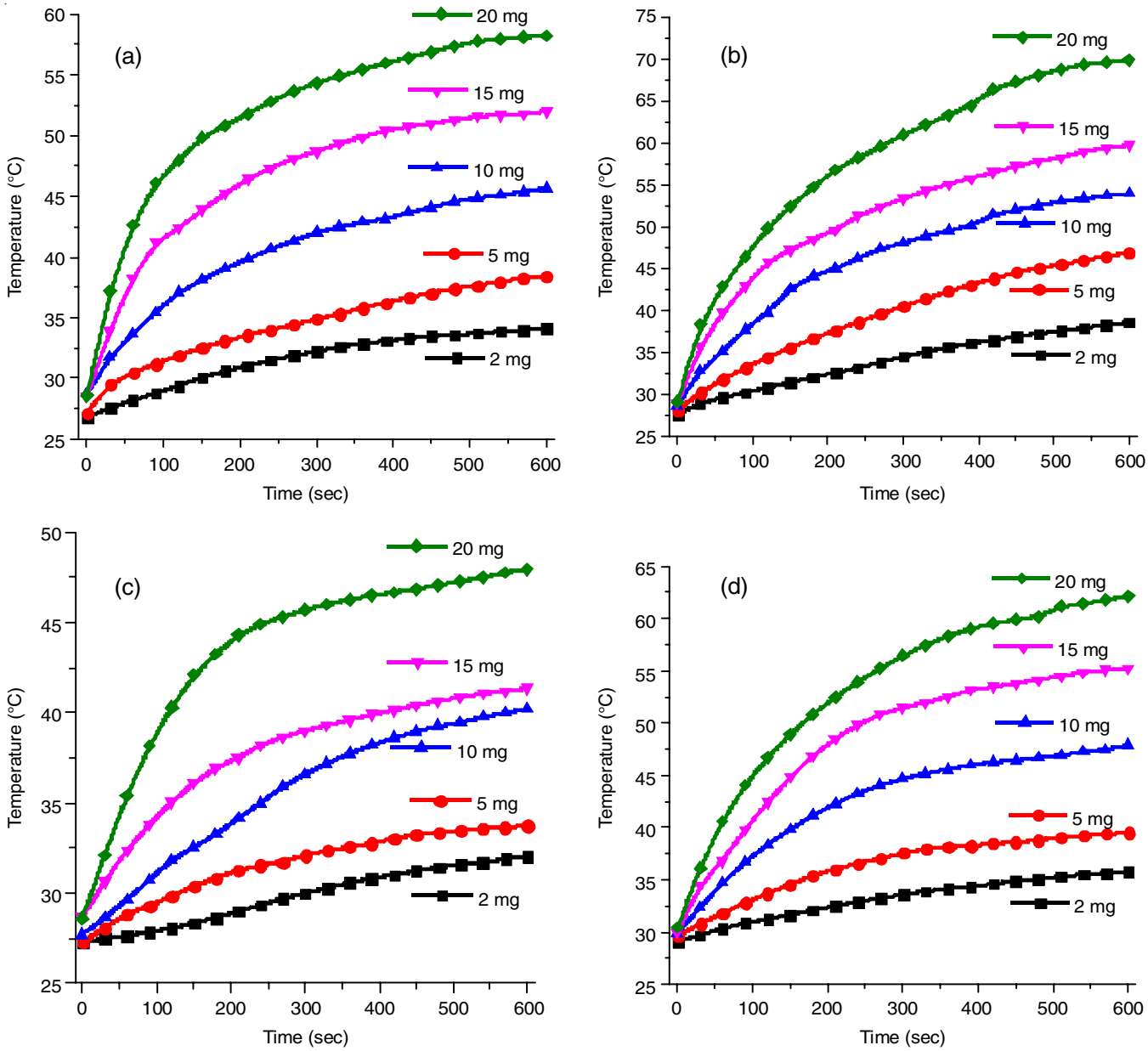

Fig. 5. Induction heating profiles for different concentrations (2-20 mg/mL) of the samples: (a) Fe_3O_4 at 200 A; (b) Fe_3O_4 at 300 A; (c) Fe_3O_4@$GdVO_4$:Eu^{3+} at 200 A and (d) Fe_3O_4@$GdVO_4$:Eu^{3+} at 300 A

and 5 mg samples are also not able to achieve hyperthermia temperature. However, it is found that 10, 15 and 20 mg concentration can be beneficial for hyperthermia temperature and time dependent target drug delivery. Keeping into consideration the dose, time of exposure and magnetic field strength will be key factors to enhance the heating and killing of tumors with minimal invasiveness and therefore will not cause thermal ablation of the cells and tissue in the vicinity of target.

Photoluminescence study: Fig. 6 shows the excitation spectrum of the Fe_3O_4@$GdVO_4$:Eu^{3+} nanocomposite. The emission wavelength is monitored at 615 nm of Eu^{3+}. A strong excitation band is observed at about 300 nm corresponding to the spin allowed $^1A_2(^1T_1)\rightarrow{}^1A_1(^1E)$ charge transfer (CT) transitions in VO_4 group. The excitation peaks of Eu^{3+} are not observed as the CT excitation is very intense. Fig. 6b shows the emission spectrum of Fe_3O_4@$GdVO_4$:Eu^{3+} nanocomposite after excitation at 300 nm. The spectrum exhibits emission bands at 540 ($^5D_1\rightarrow{}^7F_1$), 560 ($^5D_1\rightarrow{}^7F_2$), 581 ($^5D_0\rightarrow{}^7F_0$), 595 ($^5D_0\rightarrow{}^7F_1$), 615 ($^5D_0\rightarrow{}^7F_2$), 652 ($^5D_0\rightarrow{}^7F_3$) and 710 ($^5D_0\rightarrow{}^7F_4$) nm [18]. Among these, the emission at 615 nm is the strongest and the nanocomposite sample gives red light. Here, since the nanocomposite sample contains only Eu^{3+} as lanthanide emitter, the ultraviolet radiation is used to excite the sample as a model probe. However, the luminescent component can be replaced by an upconversion phosphor and the infrared radiation will be applicable for excitation and can be more beneficial for non-invasive imaging applications.

***In vitro* cell viability studies:** The *in vitro* biocompatibility profiles of Fe_3O_4@$GdVO_4$:Eu^{3+} nanocomposite are shown in Fig. 7. The Fe_3O_4@$GdVO_4$:Eu^{3+} nanocomposite shows high

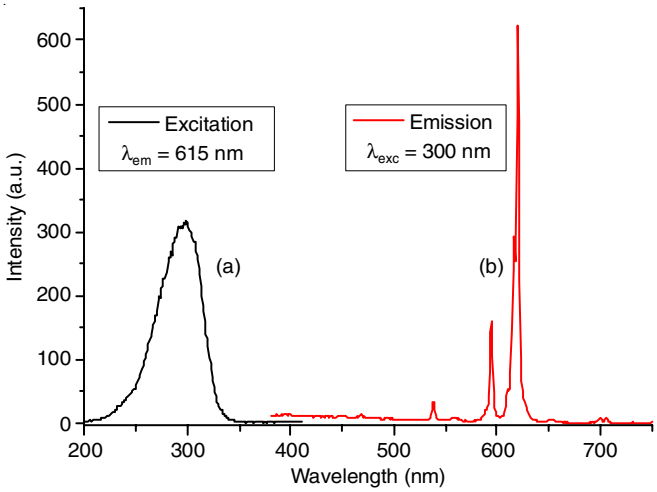

Fig. 6. Excitation (a) and emission (b) spectra of the Fe_3O_4@$GdVO_4$:Eu^{3+} sample

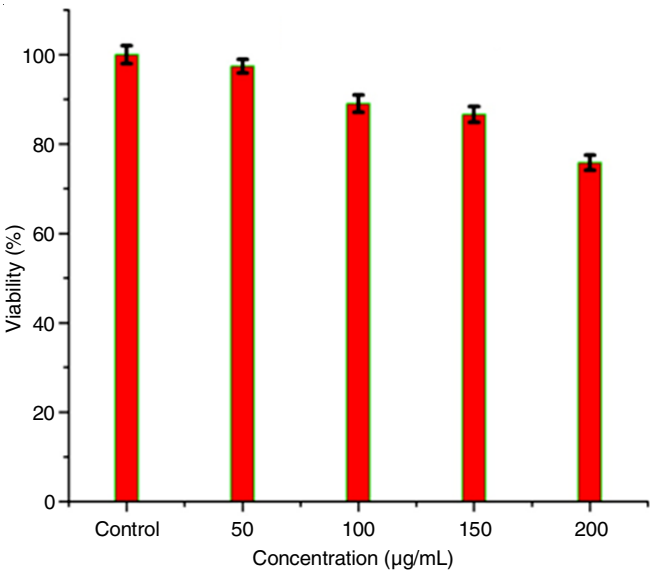

Fig. 7. Biocompatibility profiles of the Fe_3O_4@$GdVO_4$:Eu^{3+} nanocomposite

viability in HCT116 cell and the viability of cell decreases with increasing concentration of nanocomposite. It can have viability up to 75.82% for 200 µg/mL.

Conclusion

In this work, an novel magnetic materials Fe_3O_4@$GdVO_4$:Eu^{3+} nanocomposite emitting red light was prepared to investigate its capacity for heat generation when subjected to alternating magnetic fields. The XRD analysis shows that Fe_3O_4 crystallized in a cubic structure whereas the mixed phase of cubic and tetragonal structure was observed for Fe_3O_4@$GdVO_4$:Eu^{3+} nanocomposite. From the FTIR study, it is observed that the prepared nanoparticles and nanocomposite were well capped by PEG 400 as solvent medium and capping agent. TEM images of the Fe_3O_4@$GdVO_4$:Eu^{3+} nanocomposite consist of particles of mainly two different sizes-one with smaller dimensions of less than 10 nm for Fe_3O_4 nanoparticles and another of nearly 100 nm in size for $GdVO_4$:Eu^{3+} nanocomposite. From the hyperthermia study, Fe_3O_4 and Fe_3O_4@$GdVO_4$:Eu^{3+} exhibit high heating efficiency. The magnetization values for Fe_3O_4 and Fe_3O_4@$GdVO_4$:Eu^{3+} were found to be 56.52 +emu/g and 24.09 emu/g, respectively. The photoluminescence properties of Fe_3O_4@$GdVO_4$:Eu^{3+} was carried out which shows a strong red emission at 615 nm after exciting at the host (VO_4 group). From the above results, it can be concluded that the prepared samples represent an attractive nanoscale platform for a variety of applications that rely on magnetic fluid hyperthermia. The synthesized samples are found to be highly compatible with blood with less than 5% hemolysis. It is worth mentioning that the results are significantly safe for biomedical applications.

ACKNOWLEDGEMENTS

The authors are grateful to SAIF, NEHU Shillong for the TEM facility; CIF, IIT Guwahati for the VSM facility, SAIF, IIT Madras for ICP-OES facility, and Dr. David Thiyam, NIT, Manipur, India for FT-IR and photoluminescence facilities.

CONFLICT OF INTEREST

The authors declare that there is no conflict of interests regarding the publication of this article.

REFERENCES

1. Y. Ling, X. Tang, F. Wang, X. Zhou, R. Wang, L. Deng, T. Shang, B. Liang, P. Li, H. Ran, Z. Wang, B. Hu, C. Li, G. Zuo and Y. Zheng, *RSC Adv.*, **7**, 2913 (2017); https://doi.org/10.1039/C6RA20860F
2. J. van der Zee, *Ann. Oncol.*, **13**, 1173 (2002); https://doi.org/10.1093/annonc/mdf280
3. S.K. Sharma, N. Shrivastava, F. Rossi, L.D. Tung and N.T.K. Thanh, *Nano Today*, **29**, 100795 (2019); https://doi.org/10.1016/j.nantod.2019.100795
4. R. Ivkov, *Int. J. Hyperthermia*, **29**, 703 (2013); https://doi.org/10.3109/02656736.2013.857434
5. C.S.S.R. Kumar and F. Mohammad, *Adv. Drug Deliv. Rev.*, **63**, 789 (2011); https://doi.org/10.1016/j.addr.2011.03.008
6. S. Huang, Z. Cheng, P. Ma, X. Kang, Y. Dai and J. Lin, *Dalton Trans.*, **42**, 6523 (2013); https://doi.org/10.1039/c3dt33114h
7. L. Wang, H. Zhang, Z. Zhou, B. Kong, L. An, J. Wei, H. Yang, J. Zhao and S. Yang, *J. Mater. Chem. B Mater. Biol. Med.*, **3**, 1433 (2015); https://doi.org/10.1039/C4TB01981D
8. S.S. Yi, J.S. Bae, K.S. Shim, B.K. Moon, H.J. Seo, J.H. Jeong and J.H. Kim, *J. Alloys Compd.*, **408-412**, 890 (2006); https://doi.org/10.1016/j.jallcom.2004.12.107
9. B.P. Singh, A.K. Parchur, R.S. Ningthoujam, A.A. Ansari, P. Singh and S.B. Rai, *Dalton Trans.*, **43**, 4770 (2014); https://doi.org/10.1039/C3DT52786G
10. S. Laurent, S. Dutz, U.O. Häfeli and M. Mahmoudi, *Adv. Colloid Interface Sci.*, **166**, 8 (2011); https://doi.org/10.1016/j.cis.2011.04.003
11. R. Priya, O.P. Pandey and S.J. Dhoble, *Optics Laser Technol.*, **135**, 106663 (2021); https://doi.org/10.1016/j.optlastec.2020.106663
12. C. Cao, W. Qin, J. Zhang, Y. Wang, P. Zhu, G. Wei, G.Wang, R. Kim and L. Wang, *Optics Lett.*, **33**, 857 (2008); https://doi.org/10.1364/OL.33.000857
13. N. Kumam, L.P. Singh, S.K. Srivastava and N.R. Singh, *J. Lumin.*, **203**, 59 (2018); https://doi.org/10.1016/j.jlumin.2018.05.058
14. G.S. Ningombam, R.S. Ningthoujam, S.N. Kalkura and N.R. Singh, *J. Phys. Chem. B*, **122**, 6862 (2018); https://doi.org/10.1021/acs.jpcb.8b02364

15. M. Regueiro-Figueroa, S. Gündüz, V. Patinec, N.K. Logothetis, D. Esteban-Gómez, R. Tripier, G. Angelovski and C. Platas-Iglesias, *Inorg. Chem.*, **54**, 10342 (2015); https://doi.org/10.1021/acs.inorgchem.5b01719
16. H. Li and T.J. Meade, *J. Am. Chem. Soc.*, **141**, 17025 (2019); https://doi.org/10.1021/jacs.9b09149
17. K. Fukuda, S. Fujieda, K. Shinoda, S. Suzuki and B. Jeyadevan, *J. Phys.: Conf. Ser.*, **352**, 012020 (2012); https://doi.org/10.1088/1742-6596/352/1/012020
18. P. Caravan, C.T. Farrar, L. Frullano and R. Uppal, *Constrat Media Mol. Imaging*, **4**, 89 (2009); https://doi.org/10.1002/cmmi.267
19. S. Laurent, D. Forge, M. Port, A. Roch, C. Robic, L. Vander Elst and R.N. Muller, *Chem. Rev.*, **108**, 2064 (2008); https://doi.org/10.1021/cr068445e
20. S. Mornet, S. Vasseur, F. Grasset and E. Duguet, *J. Mater. Chem.*, **14**, 2161 (2004); https://doi.org/10.1039/b402025a
21. E. Katz and I. Willner, *Angew. Chem. Int. Ed.*, **43**, 6042 (2004); https://doi.org/10.1002/anie.200400651
22. T. Matsunaga, Y. Okamura and T. Tanaka, *J. Mater. Chem.*, **14**, 2099 (2004); https://doi.org/10.1039/b404844j
23. A. Rajan, M. Sharma and N.K. Sahu, *Sci. Rep.*, **10**, 15045 (2020); https://doi.org/10.1038/s41598-020-71703-6
24. E.M. Materón, C.M. Miyazaki, O. Carr, N. Joshi, P.H.S. Picciani, C.J. Dalmaschio, F. Davis and M. Flavio, *Appl. Surf. Sci. Adv.*, **6**, 100163 (2021); https://doi.org/10.1016/j.apsadv.2021.100163
25. T. Kim, E.J. Cho, Y. Chae, M. Kim, A. Oh, J. Jin, E.S. Lee, H. Baik, S. Haam, J.S. Suh, Y.M. Huh and K. Lee, *Angew. Chem. Int. Ed.*, **50**, 10589 (2011); https://doi.org/10.1002/anie.201103108
26. M. Peiravi, H. Eslami, M. Ansari and H. Zare-Zardini, *J. Indian Chem. Soc.*, **99**, 100269 (2022); https://doi.org/10.1016/j.jics.2021.100269
27. T. Mosmann, *J. Immunol. Methods*, **65**, 55 (1983); https://doi.org/10.1016/0022-1759(83)90303-4
28. J. Beik, Z. Abed, F.S. Ghoreishi, S. Hosseini-Nami, S. Mehrzadi, A. Shakeri-Zadeh and S.K. Kamrava, *J. Control. Release*, **235**, 205 (2016); https://doi.org/10.1016/j.jconrel.2016.05.062
29. A. Hajalilou, L.P. Ferreira, M.E. Melo Jorge, C.P. Reis and M.M. Cruz, J. Magnet. Magn. Mater., 537, 168242 (2021); https://doi.org/10.1016/j.jmmm.2021.168242
30. A. Alkhayal, A. Fathima, A.H. Alhasan and E.H. Alsharaeh, *Nanomaterials*, **11**, 2398 (2021); https://doi.org/10.3390/nano11092398
31. G.S. Ningombam, D. Chattopadhyay, K. Sarkar, S.N. Kalkura and N.R. Singh, *Colloids Surf. A Physicochem. Eng. Asp.*, **625**, 126826 (2021); https://doi.org/10.1016/j.colsurfa.2021.126826
32. G.S. Ningombam, B. Srinivasan, A.H. Chidananda, S.N. Kalkura, Y. Sharma and N.R. Singh, *Dalton Trans.*, **51**, 8510 (2022); https://doi.org/10.1039/D2DT00308B
33. C.A. Quinto, P. Mohindra, S. Tong and G. Bao, *Nanoscale*, **7**, 12728 (2015); https://doi.org/10.1039/C5NR02718G
34. B.K. Sodipo and A.A. Aziz, *J. Magn. Magn. Mater.*, **416**, 275 (2016); https://doi.org/10.1016/j.jmmm.2016.05.019
35. Q. Zeng, I. Baker, J.A. Loudis, Y. Liao, P.J. Hoopes and J.B. Weaver, *Appl. Phys. Lett.*, **90**, 233112 (2007); https://doi.org/10.1063/1.2746064
36. A.I. Prasad, A.K. Parchur, R.R. Juluri, N. Jadhav, B.N. Pandey, R.S. Ningthoujam and R.K. Vatsa, *Dalton Trans.*, **42**, 4885 (2013); https://doi.org/10.1039/c2dt32508j
37. X.L. Liu, H.M. Fan, J.B. Yi, Y. Yang, E.S.G. Choo, J.M. Xue, D.D. Fan and J. Ding, *J. Mater. Chem.*, **22**, 8235 (2012); https://doi.org/10.1039/c2jm30472d